J Fail. Anal. and Preven. (2018) 18:1635–1642
https://doi.org/10.1007/s11668-018-0563-9

TECHNICAL ARTICLE—PEER-REVIEWED

Reliability and Failure Analysis of Jet Vane TVC System

N. Raouf · Seid H. Pourtakdoust · S. Samiei Paghaleh

Submitted: 26 November 2017 / Published online: 12 November 2018

Abstract Structural and system reliability of a typical jet vane (JV) thrust vector control (TVC) subsystem subjected to stochastic loadings is investigated. Jet vane TVC (JVTVC) is used in many aerospace liquid and solid propulsion systems. For the purpose of this work, JVTVC structural reliability of a solid rocket propulsion system is computed using an explicit closed-form limit state function. The JV structure is influenced by the internal ballistic loads emanating out of the solid rocket propulsion internal ballistic, whose performance is modeled via a one-dimensional uniform flow assumption at the engine steady operating condition. Subsequently, JV structural reliability is predicted using the methods of mean value first-order second-moment as well as the first- and second-order reliability methods. The reliability results of the analytical methods are compared with Monte Carlo simulation for verification purposes. Finally, a comprehensive sensitivity analysis is performed to identify the key JVTVC and solid rocket propulsion design parameters affecting the TVC total system reliability. The parameters considered for sensitivity analysis include the JV geometric and structural properties as well as the solid rocket propulsion ballistic and geometric features. It turned out that the vane support arm radius and the vane area are the most important strength and load design variables, respectively, that impact the JVTVC failure reliability.

Keywords Jet vane · Structural reliability · FORM · Failure probability · TVC

N. Raouf · S. H. Pourtakdoust (✉) · S. Samiei Paghaleh
Center for Research and Development in Space Science and Technology, Sharif University of Technology, Tehran 11365-9567, Iran
e-mail: pourtak@sharif.edu

Introduction

Reliability is considered as an important measure of operational quality for high-technology systems and industries such as aerospace. The reliability of a jet vane-type thrust vector control (TVC) subsystem is investigated in the current study. TVC is utilized as an alternative to aerodynamic control surface in many aerospace solid and liquid propulsion systems. Structural and system reliability of TVCs is of importance as its failure renders the total mission useless. There are three categories of TVC systems used for thrust reorientation that include gimbaled nozzle, secondary injection and mechanical jet vane deflection [1]. The jet vane TVC (JVTVC) is the most common and convenient system among TVCs due to its simpler mechanism, smaller size and lower cost. Besides, it can also provide three-axis controls that are absent in gimbaled TVC. JVTVC is typically placed in the nozzle aft section of the propulsion systems for rapid maneuvering and active flight path control [2]. Figure 1 demonstrates the superiority of JVTVC over conventional aerodynamic controlled surfaces for pitch maneuvering [3]. Internal JVTVCs are subjected to engine exhaust flow that comprises of heavy mechanical as well as thermal loads during operation. There are uncertainties involved in both the propulsion system exhaust gas flow and the JVTVC system parameters that affect its structural reliability. In this sense, structural reliability reflects the probability that the JV structure will not fail while performing its task for accurate flight path control. Although traditional structural design utilizes the concept of load-based safety factor, the load and strength distributions are simultaneously considered in reliability-based structural design approach [4, 5]. This is important,

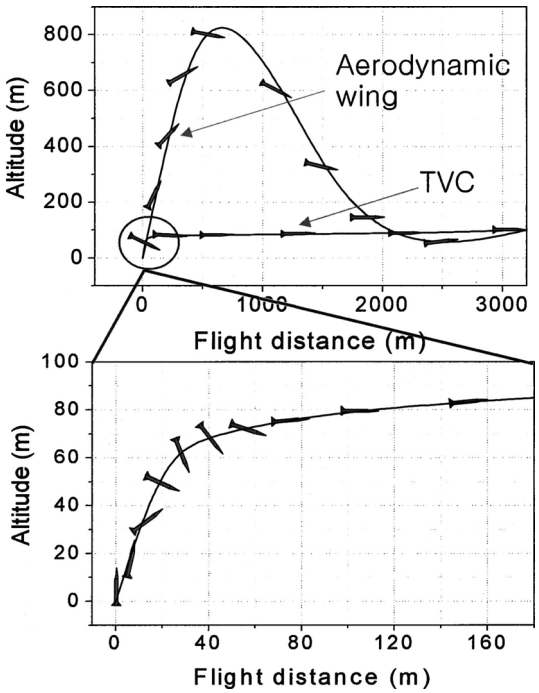

Fig. 1 Comparison of pitch maneuver between jet vane TVC and aerodynamic control [3]

as the safety factor-based design potentially increases the structural weight.

Also among the related existing literature, there are a few studies focused on erosion and ablation modeling of JV that emanates out of their interaction with the hot combustion gases [6, 7] and address the design issues as well as prediction of forces produced by the jet vanes [8]. Solid rocket motor (SRM) and launch vehicle structural reliability have also been investigated by the current authors [9, 10]. The current study covers static structural reliability analysis of jet vane TVCs at critical operating condition, using analytical techniques via an explicit limit state function (LSF) where structural reliability is verified using Monte Carlo simulation. The work concludes by a safety factor computation and a complete sensitivity analysis that identifies the JV key design parameters affecting its reliability. The remaining parts of this paper are arranged as follows. "Load Analysis and JV Structural Modeling" section details out the jet vane load analysis, structural modeling and specifications. "Reliability Analysis" section describes the theory of reliability and different related techniques. A comprehensive sensitivity analysis is given in "Sensitivity Analysis" section, followed by a discussion of results and conclusions in "Discussion of Results" and "Conclusions" sections, respectively.

Load Analysis and JV Structural Modeling

The basic principle behind the determination of JV forces is similar to that of supersonic wings. Assuming isentropic, steady one-dimensional supersonic flow, the vane normal force can be computed as [11],

$$N = \frac{1}{2}\rho v^2 S C_N \quad \text{(Eq 1)}$$

where ρ and v are the nozzle exit density and velocity, respectively, and S is the vane area. For a thin vane of arbitrary shape in two-dimensional supersonic flow, linearized aerodynamic theory provides the normal force coefficient as,

$$C_N = \frac{4\alpha}{\sqrt{M^2 - 1}} \quad \text{(Eq 2)}$$

where α represents the vane angle of attack and/or deflection in radians that is taken at its maximum for reliability analysis and M is the nozzle exit Mach number. Two-dimensional results are usually corrected via an aerodynamic correction factor η that yields an improved approximate 3D value for the normal force coefficient [2, 3]. Substituting Eq 2 into Eq 1 results in the total normal applied force on the vane as

$$N = \frac{2\rho v^2 S \eta \alpha}{\sqrt{M^2 - 1}} \quad \text{(Eq 3)}$$

The nozzle exit gas properties (M, v, ρ) at the vane location can be calculated analytically using gas dynamic theory and nozzle flow relations. The exit flow Mach number can be computed from the famous implicit *area–Mach number relation* [11],

$$\frac{A_e}{A_t} = \frac{1}{M}\left[\frac{2}{\gamma+1}\left(1 + \frac{\gamma-1}{2}M^2\right)\right]^{\frac{\gamma+1}{2(\gamma-1)}} \quad \text{(Eq 4)}$$

where A_e and A_t are the cross-sectional area of the nozzle exit and nozzle throat, respectively, and γ is the isentropic parameter (ratio of specific heats). The nozzle exit velocity can also be calculated as,

$$v = M\sqrt{\gamma R T} \quad \text{(Eq 5)}$$

where $\sqrt{\gamma R T}$ is the speed of sound, R is the exhaust gas constant, and T represents the nozzle exit flow temperature that can be determined from an isentropic relation

$$\frac{T_0}{T} = 1 + \frac{\gamma - 1}{2}M^2 \quad \text{(Eq 6)}$$

where T_0 is the chamber stagnation temperature. Again, Substituting Eq 6 into Eq 5 yields the final expression for flow velocity at the vane location.

$$v = M\sqrt{\frac{\gamma RT_0}{1+\frac{\gamma-1}{2}M^2}} \quad \text{(Eq 7)}$$

Additionally, the nozzle exit gas flow density can be computed from the following equation,

$$\rho = \frac{P}{RT} \quad \text{(Eq 8)}$$

where P is the gas flow pressure at the nozzle exit that can be also computed by,

$$\frac{P_0}{P} = \left(1+\frac{\gamma-1}{2}M^2\right)^{\frac{\gamma}{\gamma-1}} \quad \text{(Eq 9)}$$

where P_0 is the SRM combustion chamber pressure. Thus, substituting Eqs 6 and 9 into Eq 8 yields the nozzle exit density as,

$$\rho = \frac{P_0}{RT_0\left(1+\frac{\gamma-1}{2}M^2\right)^{\frac{1}{\gamma-1}}} \quad \text{(Eq 10)}$$

Putting it all together, i.e., substituting Eqs 7 and 10 into Eq 3, results in the net normal applied force on the JV,

$$N = \frac{2S\eta\alpha P_0\gamma M^2}{\sqrt{M^2-1}\left(1+\frac{\gamma-1}{2}M^2\right)^{\frac{\gamma}{\gamma-1}}} \quad \text{(Eq 11)}$$

where the exit flow Mach number can be computed using the nozzle geometric characteristics via Eq 4. Figure 2 shows a set of four JVs arranged in cross formation. For three-axis control purposes, at least three jet vanes are needed that make a 3 out of 4 systems from the reliability point of view. Further, if the jet vanes are assumed identical and independent, the JVs system failure probability will be equal to [12]:

$$p_{f_{\text{system}}} = 1-\left(4(1-p_f)^3-3(1-p_f)^4\right) \quad \text{(Eq 12)}$$

where p_f denotes a single vane failure probability that will be subsequently computed.

The vane support arms (VSA) are usually under shear loads, bending and torsional moments. While the shear load and the torsion moment are constant throughout the arm span, its bending moment will vary with the spanwise location with a maximum value that occurs at the base (supported end). Figure 3 illustrates the shear force N, bending M_a and torsion moment T_a at a typical section of the vane.

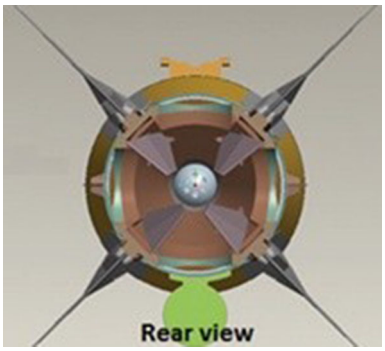

Fig. 2 Typical jet vane TVC located at the nozzle exit of SRM

Note that z-axis is parallel to the resultant force exerted on the jet vane and the x-axis is parallel to vane axis of rotation. The maximum shear stress due to the normal load N occurs along CC' and given by [13],

$$\tau_N = \frac{4N}{3A} \quad \text{(Eq 13)}$$

where $A = \pi r^2$ is the cylindrical VSA cross-sectional area of radius r. The JVTVCs are assumed to be initially symmetric about the axis of rotation (x-axis); however, due to erosion, ablation and also fabrication uncertainties, their center of pressure location, y_{CP}, will not necessarily be zero during flight. Thus, one can assume y_{CP} to be zero mean random variable (RV) with pre-specified experimental-based variance. In this sense, the torsional moment about the x-axis of rotation will be:

$$T_a = Ny_{C.P} \quad \text{(Eq 14)}$$

Moreover, the maximum shear stress due to tensional moment T_a occurs at the circumference of the cylindrical VSA that is,

$$\tau_T = \frac{T_a r}{J} \quad \text{(Eq 15)}$$

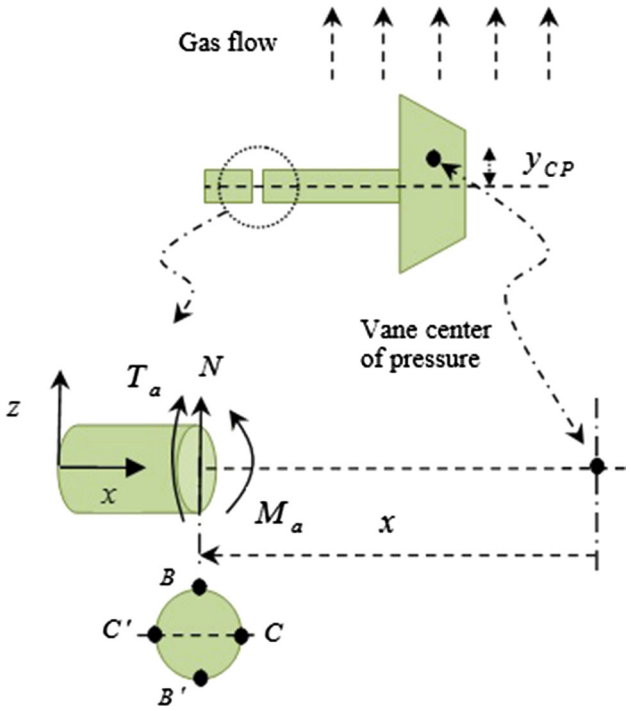

Fig. 3 Load and sign conventions at a typical section of the vane support arm

where $J = \pi r^4/2$ is the VSA polar moment of inertia that is tangent to the circumference of the VSA. Finally, the total maximum shear stress occurs at point C or C' and is a combination of both shear stresses discussed above,

$$\tau_{\max} = \frac{Ny_{C.P}r}{J} + \frac{4N}{3\pi r^2} \quad \text{(Eq 16)}$$

On the contrary, maximum bending stress occurs at the top or the bottom of the cylindrical VSA (points B or B') and calculated as,

$$\sigma_{M_a,max} = \frac{M_a r}{I} \quad \text{(Eq 17)}$$

where $M_a = Nx$ is the sectional bending moment whose maximum values occur for $x_{C.P}$, that is the distance between vane center of pressure and VSA base, and $I = \pi r^4/4$ is the VSA area moment of inertia. Failure occurs when the von Mises stress exceeds a specified threshold value governed by the material type. In turn, von Mises in a three-dimensional stress condition is computed as [13],

$$\sigma_v = \frac{1}{\sqrt{2}}\left[(\sigma_x - \sigma_y)^2 + (\sigma_y - \sigma_z)^2 + (\sigma_z - \sigma_x)^2 + 6\left(\tau_{xy}^2 + \tau_{yz}^2 + \tau_{zx}^2\right)\right]^{1/2} \quad \text{(Eq 18)}$$

where σ_x, σ_y, σ_z, τ_{xy}, τ_{yz} and τ_{zx} are typical components of stress whose values could depend on some basic random variables $\mathbf{x}$ reflecting geometric and structural properties as well as TVCs load uncertainties. Subsequently, substitution of Eqs 15 and 17 into Eq 18 gives the maximum von Mises stress at point B (or B') as,

$$\sigma_{v_{B,B'}} = \left[\left(\frac{Nx_{C.P}r}{I}\right)^2 + 3\left(\frac{Ny_{C.P}r}{J}\right)^2\right]^{1/2} \quad \text{(Eq 19)}$$

And similarly, substitution of Eq (16) into Eq (18) gives the maximum von Mises stress at point C (or C').

$$\sigma_{v_{C,C'}} = \sqrt{3}\left[\frac{Ny_{C.P}r}{J} + \frac{4N}{3\pi r^2}\right] \quad \text{(Eq 20)}$$

Finally, the failure due to yielding of a three-dimensional continuum according to the von Mises yield criterion occurs based on violation of a newly defined limit state function (LSF), i.e., $g(\mathbf{x}) < 0$

$$g(\mathbf{x}) = \sigma_t - \max[\sigma_{v_{B,B'}}, \sigma_{v_{C,C'}}] \quad \text{(Eq 21)}$$

where $\sigma_t(\mathbf{x})$ represents the TVC material allowable stress. In reality and as mentioned above, there are always some uncertainties associated with the JVTVC system design variables in terms of geometry, material and ballistic properties of SRM that are characterized in Table 1. Please note that coefficient of variation (COV) of the design RVs can be usually selected by an expert designer or determined via available experimental data.

Reliability Analysis

The structural failure probability is defined as [23]

$$p_f = P(g(\mathbf{x}) < 0) = \int_{g(\mathbf{x}) < 0} f_{\mathbf{x}}(\mathbf{x})\mathrm{d}\mathbf{x} \quad \text{(Eq 22)}$$

where $f_X(\mathbf{x})$ is the joint probability density function (PDF) of random variables $\mathbf{x}$ and the integration is to be performed over the failure domain $g(\mathbf{x}) < 0$. For many practical applications, $g(\mathbf{x})$ is a highly nonlinear function of $\mathbf{x}$ consisting of numerous RVs. In these cases exact numerical integration of Eq 22 is an impractical task. Therefore, several approximate methods have been developed. A possible approach with acceptable accuracy will be via Monte Carlo simulation (MCS) by utilizing a large number of samples [14]. As the direct Monte Carlo method is usually time-consuming, there is a tendency toward

Table 1 Jet vane and SRM design RVs characteristics

Random variables	Unit	μ	COV (%)	Distribution type
Nozzle throat diameter, D_t	m	0.35	5	Bounded normal
Nozzle exit diameter, D_e	m	1.2	5	Bounded normal
Vane area, S	m2	0.06	1	Bounded normal
Isentropic parameter, γ	⋯	1.18	5	Bounded normal
Chamber pressure, P_0	MPa	8.0	5	Bounded normal
Aerodynamic correction factor, η	⋯	0.75	1	Bounded normal
Tensile strength, σ_t	MPa	300	0.66	Bounded normal
Vane center of pressure, $x_{C.P}$	m	0.15	5	Bounded normal
Vane center of pressure, $y_{C.P}$	m	0	$\sigma = 0.01$	Bounded normal
Vane angle of attack, α	deg	15.0	1	Bounded normal
Vane arm radius, r	m	0.02	1	Bounded normal

analytical approximation methods such as the first- and second-order reliability methods (FORM and SORM) [15].

Mean Value First-Order Second-Moment Method

Computation of multiple integrals in Eq 21 requires $f_X(\mathbf{x})$ over all of the jet vane and SRM design RVs that are seldom accessible. However, the mean and standard deviation of individual RVs are usually known to a logically acceptable degree of precision. In this way, mean value first-order second-moment (MVFOSM) provides an approximation for reliability via first-order Taylor series expansion of LSF around the mean values of the RVs. The MVFOSM reliability index β is described as [16].

$$\beta = \frac{g(\boldsymbol{\mu}_{\mathbf{x}})}{\sqrt{(\nabla_{\mathbf{x}} g)^T_{\mathbf{x}=\boldsymbol{\mu}_{\mathbf{x}}} \boldsymbol{\Sigma}_{xx} (\nabla_{\mathbf{x}} g)_{\mathbf{x}=\boldsymbol{\mu}_{\mathbf{x}}}}} \quad \text{(Eq 23)}$$

where $\boldsymbol{\mu}_{\mathbf{x}}$ and $\boldsymbol{\Sigma}_{xx}$ are the mean and covariance matrix of $\mathbf{x}$ and $\nabla_{\mathbf{x}} g$ is the gradient vector of the $g(\mathbf{x})$ with respect to the $\mathbf{x}$. Moreover, for $p_f < 0.5$, probability of failure is found by

$$p_f \approx \Phi(-\beta) \quad \text{(Eq 24)}$$

where Φ is the standard normal cumulative distribution function.

First-Order Reliability Method

FORM is one of the most common and reliable techniques of structural reliability estimation. In this method, the following optimization problem must be solved in the independent standard normal space U [22].

$$\min_{\mathbf{u}} \|\mathbf{u}\| = \sqrt{\sum_{i=1}^{n} u_i^2} \quad \text{subject to } g(\mathbf{u}) = 0 \quad \text{(Eq 25)}$$

where $\|\cdot\|$ stands for the norm of a vector and $g(\mathbf{u})$ is the LSF in the U space. The solution of Eq 25 is called design point or most probable point and denoted by $\mathbf{u}^*$, and accordingly, the reliability index will be $\beta = \|\mathbf{u}^*\|$. Again for $p_f < 0.5$, p_f is found by Eq 23. To solve Eq 25, various algorithms such as Hasofer–Lind and Rackwitz–Fiessler (HLRF) [15, 17] and improved HLRF (iHLRF) algorithm [18] are developed.

Second-Order Reliability Method

When the LSF is highly nonlinear, the SORM may be more accurate than the FORM. The SORM utilizes a second-order approximation of the LSF around the design point. Breitung derived the following formulation for the approximation of the SORM [19],

$$p_f \approx \Phi(-\beta) \prod_{i=1}^{n-1} \frac{1}{\sqrt{1+\beta\kappa_i}} \quad \text{(Eq 26)}$$

where β is found via FORM and n is the number of basic variables. In Eq 26 κ_i, $i = 1, \ldots, n-1$ denotes principal curvatures of the $g(\mathbf{u})$ at the design point. To compute the main curvatures κ_i, the following symmetric matrix must be calculated [20]

$$B = \frac{PHP^T}{\|\nabla_{\mathbf{u}} G(\mathbf{u}^*)\|} = \begin{bmatrix} B_{11} & B_{12} \\ B_{12}^T & b_{nn} \end{bmatrix} \quad \text{(Eq 27)}$$

where B_{11} is the $(n-1) \times (n-1)$ matrix formed by the first $n-1$ rows and columns of B, H is the $n \times n$ second-derivative matrix of the LSF in the standard normal space U evaluated at the $\mathbf{u}^*$, and P is the orthogonal rotation matrix which rotates $\mathbf{u}$ into a new space $\tilde{U}$, where the nth row of the rotation matrix P is α,

$$\tilde{\mathbf{u}} = P\mathbf{u}, \quad \alpha = \frac{\nabla_{\mathbf{u}} G(\mathbf{u}^*)}{\|\nabla_{\mathbf{u}} G(\mathbf{u}^*)\|} \quad \text{(Eq 28)}$$

Finally, κ_i are the eigenvalues of B_{11}.

Monte Carlo Method

MCS is also among the common methods utilized for structural reliability computation and often times as a means to validate other methods such as FORM and/or SORM. The disadvantage of MCS is the intense computational burden. Equation 22 can be written in another form as

$$p_f = \int k[g(\mathbf{x}) < 0] f_{\mathbf{x}}(\mathbf{x}) \mathrm{d}\mathbf{x} \quad \text{(Eq 29)}$$

where the integration is performed over the entire sample space and k is an indicator function defined by,

$$k[g(\mathbf{x}) < 0] = \begin{cases} 1 & \text{if } g(\mathbf{x}) < 0 \\ 0 & \text{otherwise} \end{cases} \quad \text{(Eq 30)}$$

Note that Eq 29 represents the expected value of $k[g(\mathbf{x}) < 0]$ that can be rewritten in terms of the frequency of occurrence, or in other words as:

$$p_f = \frac{1}{N_s} \sum_{i=1}^{N_s} k[g(\mathbf{x}_i) < 0] \quad \text{(Eq 31)}$$

or

$$p_{\mathrm{f}} = \frac{N_{\mathrm{f}}}{N_{\mathrm{s}}} \quad \text{(Eq 32)}$$

where N_{s} and N_{f} are the simulation number and the number of observations favoring $g(\mathbf{x}) < 0$, respectively. The

required simulation number in the direct MCS can be estimated as

$$N_s = \frac{1 - p_f}{\delta_{p_f}^2 p_f} \quad \text{(Eq 33)}$$

where δ_{p_f} is the COV of the failure probability where small values of δ_{p_f} are desirable. The direct Monte Carlo technique requires a large number of simulations to estimate the structural reliability, particularly for small values of p_f. However, the number of sample runs can be significantly reduced using some variance reduction techniques, such as directional sampling, Latin hypercube sampling, importance sampling, conditional expectation [21]. In this respect, Monte Carlo with importance sampling (MCIS) is one of the most common techniques for variance reduction in structural reliability assessment that requires less computational effort in comparison with the direct MCS. To develop the MCIS, Eq 29 can be rewritten in U space as

$$p_f = \int k[g(\mathbf{u}) < 0] \frac{\varphi_{\mathbf{u}}(\mathbf{u})}{h_{\mathbf{u}}(\mathbf{u})} h_{\mathbf{u}}(\mathbf{u}) d\mathbf{u} \quad \text{(Eq 34)}$$

where $h_{\mathbf{u}}$ is the importance sampling density function and $\varphi_{\mathbf{u}}$ is the standard normal density function in U space. Note that $h_{\mathbf{u}}$ is selected such that a large number of the samples fall inside the failure domain. In practice, $h_{\mathbf{u}}$ is chosen as a normal density function with mean values equal to the $\mathbf{u}^*$ obtained from the FORM analysis. Now Eq 34 can be interpreted as the expected value of the $k[g(\mathbf{u}) < 0] \frac{\varphi_{\mathbf{u}}(\mathbf{u})}{h_{\mathbf{u}}(\mathbf{u})}$ with respect to the importance sampling density function, thus

$$p_f = \frac{1}{N_s} \sum_{i=1}^{N_s} k[g(\mathbf{u}_i) < 0] \frac{\varphi_{\mathbf{u}}(\mathbf{u}_i)}{h_{\mathbf{u}}(\mathbf{u}_i)} \quad \text{(Eq 35)}$$

In this procedure sample points are concentrated around the design point and thus require less simulation runs as opposed to direct MCS.

Sensitivity Analysis

Sensitivity analysis can be used as a tool to improve the structural reliability of the jet vane. In the previous section, common techniques of structural reliability assessment were discussed, most of which rely on the means and variances of the design RVs. Now, if the reliability turns out to be lower than the required value, one can change the mean values or reduce the variances of the RVs to enhance the vane reliability. In this respect the sensitivity analysis is the most effective approach that identifies the key design variables affecting the jet vane reliability. It also enables one to ignore RVs that are least influencing the reliability, and as such, they could be deterministically specified in the design process. In this regard, the normalized importance vectors $\boldsymbol{\delta}$ and $\boldsymbol{\eta}$ are defined as

$$\delta_i = \frac{\partial \beta}{\partial \mu_i} \sigma_i \quad \text{(Eq 36)}$$

$$\eta_i = \frac{\partial \beta}{\partial \sigma_i} \sigma_i \quad \text{(Eq 37)}$$

where δ_i and η_i are the sensitivity of β with respect to the variations in mean and uncertainty of the RVs, respectively.

Discussion of Results

Table 2 shows a comparison of reliability results obtained via various methods discussed in "Reliability Analysis" section for single JV as well as for a set of four JVTVC. To verify the efficiency and accuracy of various reliability assessment methods, MCS and its enhancement approach of MCIS have also been implemented and reported. Please note that Table 2 includes the number of LSF evaluations N_1 as well as the number of iterations N_2 pertinent to each technique. It is observed that the analytical FORM/SORM

Table 2 Comparison of different reliability methods

Method	Single vane		N_1	N_2	Error (%)[a]	System
	β	p_f				$p_{f_{system}}$
MVFOSM	2.6643	0.00386	23	1	− 7.39	8.89×10^{-5}
FORM	2.1834	0.01450	92	4	− 2.16	0.00124
SORM (Breitung)	2.1769	0.01474	598	4	− 0.54	0.00128
Direct MCS	2.1749	0.01482	2.4×10^6	2.4×10^6	⋯	0.00129
MCIS	2.1749	0.01482	6.0×10^4	6.0×10^4	⋯	0.00129

[a]With respect to the MCS

results are compatible with Monte Carlo simulations, though MCIS needs less computational efforts. In addition, as noticeable in Table 2, FORM and SORM techniques need 92 and 598 LSF evaluations, respectively, while direct MCS convergence occurs for a large number of samplings (2.4×10^6). The failure probability error of all methods as compared with Monte Carlo is also included in Table 2, showing that SORM is more accurate than FORM. Moreover, SORM result is in good agreement with MCS with a failure probability error of less than 1.0 percent that reflects a reliability index of $\beta = 2.1769$.

For additional highlights of the current study, the MCS results are utilized to determine the PDF of maximum applied von Mises stresses, where the material strength PDF is also available from Table 1. Figure 4 shows both PDFs whose overlapping area is proportional to failure probability. Deduced from Fig. 4, one can assess the mean value of the maximum von Mises stress and its corresponding standard deviation that is 202.757 and 39.045 MPa, respectively. Similarly, the mean and standard deviation of the material strength are 300 MPa and 300×0.0066 MPa, respectively (see Table 1). Thus, the safety factor of the assumed jet vane structure can be estimated to be 1.48 that shows the importance of reliability-based structural design and its correlation with reliability analysis. If one performs similar computations for a JVTVC system having higher COVs (for example, with a 20 percent increase in all COVs of random parameters in Table 1), a failure reliability of 0.03478 will be obtained, while the safety factor remains the same as 1.48. This shows the importance of reliability analysis and that the factor of safety alone is not a good criterion for structural design as it may only cause structural overdesign.

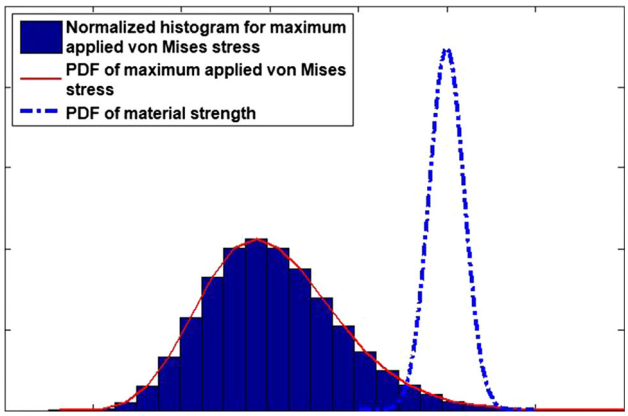

Fig. 4 PDFs of maximum applied von Mises stress and strength

Next, the reliability index sensitivity with respect to variation in means μ_{x_i} and standard deviations σ_{x_i} of all jet vane and SRM design RVs x_i is performed whose results are presented in Table 3. Note that the sign of η_i is always negative that means the structural reliability decreases with increased level of uncertainty in the design variables. The sign of δ_i identifies the variables' type, where a positive value indicates the corresponding RV as a strength-related random variable. Similarly, Table 3 indicates that nozzle exit diameter, isentropic parameter, VSA radius and the tensile strength are among the strength variables whose increase in mean values raises the JV reliability. On the other hand, the nozzle throat diameter, vane area, chamber pressure, aerodynamic correction factor, vane center of pressure and the vane angle of attack are among the load variables whose increase in mean values decreases the JV reliability. Moreover, Table 3 shows that the reliability index sensitivity is highest for the VSA radius, and thus, vane support arm radius is considered the most important

Table 3 Importance vectors

	Normalized importance vectors		Dimensional importance vectors	
Random variables	$\delta_i = \frac{\partial\beta}{\partial\mu_i}\sigma_i$	$\eta_i = \frac{\partial\beta}{\partial\sigma_i}\sigma_i$	$\frac{\partial\beta}{\partial\mu_i}$	$\frac{\partial\beta}{\partial\sigma_i}$
Nozzle throat diameter, D_t	− 0.5562	− 0.6756	− 31.7824	− 38.6058
Nozzle exit diameter, D_e	0.6338	− 0.8773	10.5632	− 14.6222
Vane area, S	− 0.0535	− 0.0063	− 89.2366	− 10.4479
Isentropic parameter, γ	0.3416	− 0.2552	5.7906	− 4.3254
Chamber pressure, P_0	− 0.2606	− 0.1485	− 0.0000	− 0.0000
Aerodynamic correction factor, η	− 0.0535	− 0.0063	− 7.1389	− 0.8358
Tensile strength, σ_y	0.0354	− 0.0027	0.0000	− 0.0000
Vane center of pressure, $x_{C.P}$	− 0.2606	− 0.1485	− 34.7504	− 19.7986
Vane center of pressure, $y_{C.P}$	− 0.0009	0	− 0.0877	0
Vane angle of attack, α	− 0.0535	− 0.0063	− 20.4515	− 2.3945
Vane arm radius, r	0.1614	− 0.0570	806.9806	− 284.7512

strength design variable impacting the jet vane reliability positively. On the contrary, the vane planform area has the most negative impact on the reliability. In this sense, one can increase the reliability by increasing the vane arm radius while reducing the vane planform area. Of course, in a realistic design process one usually should compromise between important design parameters to achieve optimum results in terms of system reliability, total weight and flight performance. The latter is beyond the scope of the current work, but the reliability indices and their help identify the key design parameters as demonstrated in Table 3. Finally, the reliability index sensitivity seems to be insignificant with respect to $y_{C.P}$, and thus, it may be considered deterministic in reliability analysis which is another advantage of performing the sensitivity analysis.

Conclusions

Structural and system reliability of a jet vane (JV) thrust vector control (TVC) system subjected to a number of uncertainties is investigated. These uncertainties are associated with the JV and solid rocket motor key design variables that include material and ballistic properties as well as some geometric characteristics. Reliability analysis is performed via a proposed explicit exact analytical limit state function (LSF) using various schemes such as first- and second-order reliability methods (FORM and SORM). In turn, the results are numerically verified with the Monte Carlo method and Monte Carlo simulation with importance sampling. Results indicate that the suggested scheme and the proposed exact LSF can be successfully utilized for reliability-based JVTVC design purposes. Moreover, a FORM-based sensitivity analysis demonstrates that the vane support arm radius and the vane area are the most important strength and load design variables, respectively, that impact the JVTVC reliability. Further research directives being conducted by authors include dynamic reliability analysis to determine time-dependent JVTVC reliability and development of a solid–fluid interaction model to determine the impact of combined fluid and thermal loads on JV structural reliability as well as failure-based system reliability computations. In this sense the current study paves the way for many more scientific researches on JV-type TVC reliability-based design and analysis.

References

1. G.P. Sutton, *Rocket propulsion elements*, 6th edn. (Wiley, New York, 1992)
2. Q.C. Québec, R. Farinaccio, R.A. Stowe. Force measurements evaluating erosion effects on jet vanes for a thrust vector control system, in 39th AIAA/ASME/SAE/ASEE Joint Propulsion Conference and Exhibit 20–23 July 2003, Huntsville, Alabama
3. Hong-Gye Sung, Yong-Seok Hwang, Thrust-vector characteristics of jet vanes arranged in x-formation within a shroud. J. Propul. Power **20**(3), 501–508 (2004)
4. I.S. Raju, D.S. Lee, M. Mohaghegh. Negative stress margins are they real?, in 52nd AIAA/ASCE/AHS/ASC Structures, Structural Dynamics, and Materials Conference, AIAA Paper 2011-1808 (2011)
5. C.E. Larsen, I.S. Raju. Moving aerospace structural design practice to a load and resistance factor approach, in 57th AIAA/ASCE/AHS/ASC Structures, Structural Dynamics, and Materials Conference, AIAA Paper 2016-0230 (2016)
6. E. Divo, A. Kassab, R. Cavalleri, Application of the DRBEM to model ablation characteristics of a thrust vector control vane. Eng. Anal. Boundary Elem. **23**(8), 693–701 (1999)
7. A.O. Danielson. Inverse heat transfer studies and the effects of propellant aluminum on TVC jet vane heating and erosion, in AIAA, SAE, ASME, and ASEE, Joint Propulsion Conference, 26th, Orlando, FL (1990)
8. C.P. Rahaim, et al. Jet vane thrust vector control: a design effort, in AIAA paper (1996): 96-2904
9. N. Raouf, S.H. Pourtakdoust, Structural reliability analysis of a solid rocket motor with ellipsoidal cap. J. Spacecr. Rockets **53**(2), 389–392 (2016)
10. N. Raouf, S.H. Pourtakdoust. Time varying structural reliability of launch vehicle via extreme response approach. J. Spacecr. Rockets 1–9 (2016)
11. J.D. Anderson, *Modern compressible flow: with historical perspective* (McGraw Hill, Boston, 2003)
12. N. Raouf, S.H. Pourtakdoust, launch vehicle multi-objective reliability-redundancy optimization using a hybrid genetic algorithm-particle swarm optimization. Proc. Inst. Mech. Eng. Part G J. Aerosp. Eng. **229**(10), 1785–1797 (2015)
13. Joseph E. Shigley, Charles R. Mischke, Richard G. Budynas, *Mechanical engineering design* (McGraw-Hill, New York, 2004)
14. Peter Bjerager, Probability integration by directional simulation. J. Eng. Mech. **114**(8), 1285–1302 (1988)
15. Abraham M. Hasofer, Niels C. Lind, Exact and invariant second-moment code format. J. Eng. Mech. Div. **100**(1), 111–121 (1974)
16. C.A. Cornell, A probability-based structural code. Am. Concr. Inst. J. Proc. **66**(12), 974–985 (1969)
17. Rüdiger Rackwitz, Bernd Flessler, Structural reliability under combined random load sequences. Comput. Struct. **9**(5), 489–494 (1978)
18. Y. Zhang, A. Der Kiureghian. Two improved algorithms for reliability analysis. In: R. Rackwitz, G. Augusti, A. Borr (eds.) Proceedings of the Sixth IFIP WG7.5 Reliability and optimization of structural systems (1995)
19. K. Breitung, Asymptotic approximations for multinormal integrals. J. Eng. Mech. **110**(3), 357–366 (1984)
20. Der Kiureghian, Hong-Zong Lin Armen, Shyh-Jiann Hwang, Second-order reliability approximations. J. Eng. Mech. **113**(8), 1208–1225 (1987)
21. S. Engelund, R. Rackwitz, A benchmark study on importance sampling techniques in structural reliability. Struct. Saf. **12**(4), 255–276 (1993)
22. Behrooz Keshtegar, Mahmoud Miri, Reliability analysis of corroded pipes using conjugate HL–RF algorithm based on average shear stress yield criterion. Eng. Fail. Anal. **46**, 104–117 (2014)
23. Hocine Dehmous, Hélène Welemane, Multi-scale reliability analysis of composite structures—application to the Laroin footbridge. Eng. Fail. Anal. **18**(3), 988–998 (2011)